Available online at www.sciencedirect.com
ScienceDirect
Ceramics International 36 (2010) 1893–1899
CERAMICS INTERNATIONAL
www.elsevier.com/locate/ceramint

The threonine effect on calcium phosphate preparation from a solution containing Ca/P = 1.33 molar ratio

K. Mahmud [a], A. Mitsionis [a], T. Vaimakis [a,*], N. Kourkoumelis [b], C. Trapalis [c]

[a] *Department of Chemistry, University of Ioannina, P.O. Box 1186, 45110 Ioannina, Greece*
[b] *Department of Medical Physics, University of Ioannina, P.O. Box 1186, 45110 Ioannina, Greece*
[c] *"Demokritos" National Centre for Scientific Research, Institute of Materials Science, 15310 Athens, Greece*

Received 12 February 2010; received in revised form 5 March 2010; accepted 20 March 2010
Available online 28 April 2010

Abstract

In this study, calcium phosphate materials were prepared by a modified precipitation method using high-speed dispersing equipment. A solution with a Ca/P molar ratio of 1.33 (octacalcium phosphate stoichiometry) was transferred into the reactor vessel with different concentrations of threonine at temperature 97 °C. A white precipitant was collected after the addition of condensed ammonium solution and the samples were subsequently calcined at 900 °C. From the XRD patterns and FT-IR spectra of the uncalcined samples, three phases of octacalcium phosphate (OCP), monetite (DCP) and hydroxyapatite (HA) were obtained. Calcined samples showed two phases of β-tricalcium phosphate (β-TCP) and calcium pyrophosphate (CPP). SEM micrographs showed the different morphology of samples. The specific surface areas (ssa) were 45–53 m^2/g for and 5–6 m^2/g for calcined samples. From the obtained results, we found that threonine added in various amounts in the initial solution inhibits the formation of HA and consequently creates OCP and DCP.

Keywords: Threonine; Calcium phosphate; Octacalcium phosphate; Hydroxyapatite

1. Introduction

Calcium phosphates are used as bone substitutes because of its high compatibility with bone tissues as well as adsorbents because of their specific adsorption properties against organic substances [1–5]. The most commonly used calcium phosphate materials are: hydroxyapatite (HA), octacalcium phosphate (OCP), monetite (DCP), tricalcium phosphate (TCP). Octacalcium phosphate ($Ca_8H_2(PO_4)_6{\cdot}5H_2O$, OCP: Ca/P molar ratio = 1.33), often occurs as a transient intermediate in the precipitation of the most thermodynamically stable hydroxyapatite ($Ca_{10}(PO_4)_6(OH)_2$, HA: Ca/P molar ratio = 1.67) [1–5], and has been suggested to be involved in the mineralization of biological tissues, such as bone and dentine [6,7]. The inorganic phase in these calcified tissues is a poor crystalline carbonated apatite, which however, could be just the final phase of a process where OCP acts as a precursor phase. Both OCP and HA are of great scientific interest in the field of biomaterials due to their importance in the formation of mineralized tissue [8]. OCP is one of the most important calcium phosphates and has a high compatibility with bone tissues. The crystalline structure of OCP is unstable and can be easily hydrolyzed to HA [9–11], so it is difficult to synthesizing pure OCP. However, it has been shown that synthetic OCP is converted into HA in vivo [12–15] and in vitro [14,16–20]. Moreover, OCP can produce HA through two possible processes [21]: the first one by hydrolysis of OCP and, the second one, by dissolution of OCP after precipitation [22,23]. It has been shown that both temperature and pH effect on the OCP stability [8,24,25]. Therefore, most of the calcium phosphate synthesis methods are carried out under exactly controlled conditions. In our present study, we controlled temperature and pH for the synthesis of calcium phosphate material. Xin et al. [26] have reported the transformation of OCP into HA by electron beam radiation in situ observations, in the transmission electron microscope (TEM) also observing OCP and HA domains as a result of a solid-state-transformation mechanism in the OCP crystals. Arellano-Jiménez et al. [27] produced OCP by precipitation and HA by direct hydrolysis of OCP. The reported intermediate system allows

* Corresponding author. Tel.: +30 2651008352; fax: +30 2651008795.
E-mail address: tvaimak@cc.uoi.gr (T. Vaimakis).

0272-8842/$36.00
doi:10.1016/j.ceramint.2010.03.027

Table 1
The experimental conditions and the specific surface area estimated from BET method and I-point method.

Sample code	Threonine concentration (mM)	After precipitation pH	Calcination	XRD phases	Specific surface area ($m^2\ g^{-1}$)	
					BET method	I-point method
TH0	0.0	8.7	No	OCP, DCP, HA	45.32	44.45
TH2	0.2	8.8	No	OCP, DCP, HA	53.12	52.09
TH4	0.4	8.9	No	OCP, DCP, HA	46.38	45.38
TH6	0.6	8.8	No	OCP, DCP, HA	48.83	47.18
TH0C	0.0		Yes	β-TCP, CPP	5.82	5.72
TH2C	0.2		Yes	β-TCP, CPP	5.76	5.49
TH4C	0.4		Yes	β-TCP, CPP	6.70	6.14
TH6C	0.6		Yes	β-TCP, CPP	6.66	6.19

studying the structural equilibrium behavior of these two phases by electron microscopy.

In our present work, we study the precipitation of phosphate materials from an initial solution with Ca/P molar ratio 1.33, which is OCP stoichiometry. The procedure we used in this work is the modified precipitation method with high-speed dispersing equipment described in our previous papers [28,29]. At the same time, we used different concentrations of threonine in order to see the effect on calcium phosphate material. Threonine is an essential amino acid, serving as a carrier for phosphate in phosphoproteins [30–32]. Threonine is present in the heart, central nervous system, and skeletal muscle. It assists in maintaining protein balance in the body and is important in the formation of collagen and elastin [33–36]. Matsumoto et al. [37] showed that the addition of amino acids such as glycine, serine, aspartic acid and glutamic acid affects on HA synthesis by changing its size, morphology and solubility. The prepared powders in our work have been studied using X-ray diffraction (XRD), Fourier transform infrared spectroscopy (FT-IR), scanning electron microscopy (SEM), differential scanning thermogravimetry–calorimetry analysis (TG–DSC) and nitrogen adsorption–desorption porosimetry.

2. Materials and methods

2.1. Chemicals

The reagents that have been used were $CaCl_2{\cdot}2H_2O$ (Fluka, Assay (KT) 99%), $Ca(H_2PO_4)_2{\cdot}H_2O$ (Riedel-de Haën, Assay 88%), threonine (Sigma, 98% TLC) and ammonia solution 25% (Riedel-de Haën).

2.2. Synthesis and characterization of calcium phosphate materials

The apparatus used is described properly in our previous works [28,29]. An 800 ml solution of 0.0538 mol of $Ca(H_2PO_4)_2{\cdot}H_2O$ and 0.0893 mol of $CaCl_2$ with a Ca/P molar ratio of 1.33 (OCP stoichiometry) were transferred into the reactor vessel and were heated to $97 \pm 1\ ^\circ C$ using an airflow rate of 15 l/h for 30 min. The rotation speed of the disperser was adjusted at 5000 rpm, and then 18 ml of concentrated NH_4OH solution (25%, w/w) was added slowly (3 min). The pH of the solution increased from 3.8 to 8.8 and white slurry was produced. The produced slurry was aged over night at room temperature, filtrated; washed using distilled water and dried at 90 °C for 6 h. The same procedure was repeated using threonine in the initial solution with concentrations of 0.2, 0.4 and 0.6 mM. A portion of the samples was subsequently calcined for 3 h at 900 °C. The calcination temperature was chosen with respect to thermal data derived from thermal analysis (TG/DSC). Table 1 shows the experimental conditions, and the sample codes for uncalcined and calcined materials.

The study of the crystal phases in the obtained products was carried out by the X-ray diffraction (XRD) technique, using a Brüker P8 Advance apparatus, with a 2θ range of 3–40° in steps of 0.02° and the identification of the patterns was made using the Powder Diffraction Files (PDF). FT-IR was performed using a spectrophotometer (Model Spectrum RX I FT-IR, PerkinElmer). The KBr disk technique was used with ~2 mg of powder in ~200 mg of spectroscopic-grade KBr (Merck), which had been dried at 100 °C. Infrared spectra were recorded in the 4000–400 cm^{-1} region.

The textural analysis of the solids was examined by N_2 adsorption–desorption porosimetry which provides also the pore size distribution, using a Fisons Instruments Sorptomatic 1900, and scanning electron microscopy (SEM), using a JEOL JSM-6300 instrument. Before N_2 adsorption–desorption measurement the sample was degassed at 150 °C and pressure of 10–30 Torr for 6 h.

Simultaneously TG/DSC (thermogravimetry/differential scanning calorimetry) measurements were carried out by a STA 449C (Netzch-Gerätebau, GmbH, Germany) equipment. The heating range was from room temperature up to 1300 °C, with a heating rate of 10 K min^{-1} under synthetic air flow rate of 30 cm^3/min. Al_2O_3 powder as reference was used.

3. Results and discussion

Fig. 1 shows the XRD patterns of uncalcined samples. All samples have been first indexed with X-cell algorithm [38] and refined afterwards with Pawley fitting in order to find the best approximation for the unit cell parameters. Background has been subtracted using a 20 points polynomial function and a smoothing function has been applied using Savitsky–Golay filter. Most of the reflection patterns were similar to the known

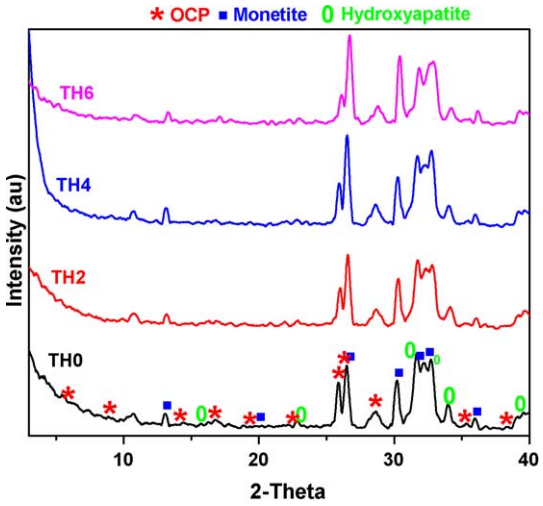

Fig. 1. XRD pattern of uncalcined samples of material.

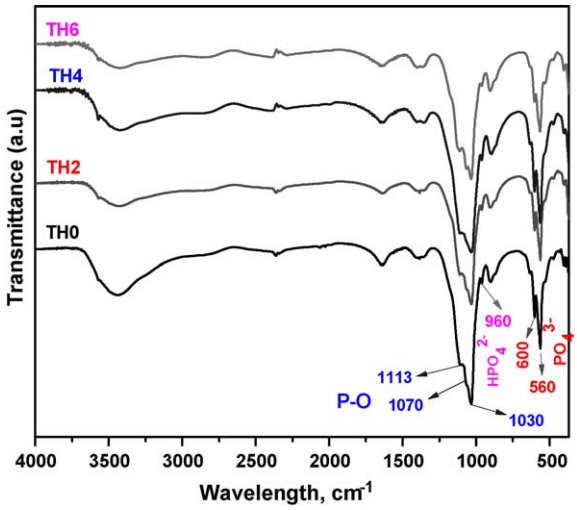

Fig. 3. FT-IR spectra of uncalcined samples of material.

reflection pattern of synthesized OCP [Powder Diffraction File 86-1407]. In the present study at first we tried to fix our crystal system as triclinic system of OCP and the calculated values of lattice parameters for OCP were $a = 7.204$ Å, $b = 6.087$ Å and $c = 4.333$ Å. However, these values do not fit with the standard triclinic system of OCP [Powder Diffraction File 26-1056]. A second thought for this crystal system was to index it as an orthorhombic system and the calculated lattice parameters for OCP were $a = 10.733$ Å, $b = 13.753$ Å and $c = 5.832$ Å. These values are more exact with standard orthorhombic OCP system [Powder Diffraction File 86-1407]. However, these values are still slightly different with standard file. This is due to the presence of multiphase on the unit cell. After using different concentrations of threonine, no change was detected in the XRD pattern of uncalcined samples. The entire pattern showed two other phases of DCP and HA. The peaks at 2θ values 4.8°, 16.7°, 22.7°, 26.0°, 26.5°, 28.6° and 36.1° derived from (0 1 0), (0 2 1), (2 0 1), (0 0 2), ($\bar{2}$ 2 1), (1 $\bar{1}$ 2) and (0 5 2) reflections indicate the phase of OCP. The peaks at 2θ values 13.0°, 30.3°, 32.5° and 32.7° derived from (0 0 1), (1 2 0), (1 0 2) and (2 0 1) planes indicate the phase of monetite [Powder Diffraction File 75-1520]. Moreover, the peaks at 2θ values 22.8°, 31.8°, 32.9° and 34.1° derived from (1 1 1), (2 1 1), (3 0 0) and (1 0 2) planes indicate the phase of hydroxyapatite [Powder Diffraction File 73-1731].

Fig. 2 shows the XRD patter of calcined samples. All the peaks detected here are very sharp. Two phases are observed here, one is β-tricalcium phosphate (β-TCP) [Powder Diffraction File 79-0700] and the other is β-calcium pyrophosphate (β-$Ca_2P_2O_7$,CPP) [Powder Diffraction File 11-177]. The lattice parameters were calculated for β-TCP, using X-cell algorithm software were, $a = 8.174$ Å, $b = 3.348$ Å and $c = 11.394$ Å. The system is monoclinic with the space group $P2/C$.

Figs. 3 and 4 show FT-IR spectra of uncalcined and calcined samples respectively. After using different concentrations of threonine, no change occurred in the band peaks for samples TH0, TH2, TH4 and TH6. The same peaks are observed in all samples. Fig. 3 shows the three distinguished bands of P–O in the orthophosphate stretch absorption appear at around 1030–1113 cm^{-1} tended to obscure the central peak at 1070 cm^{-1}. The

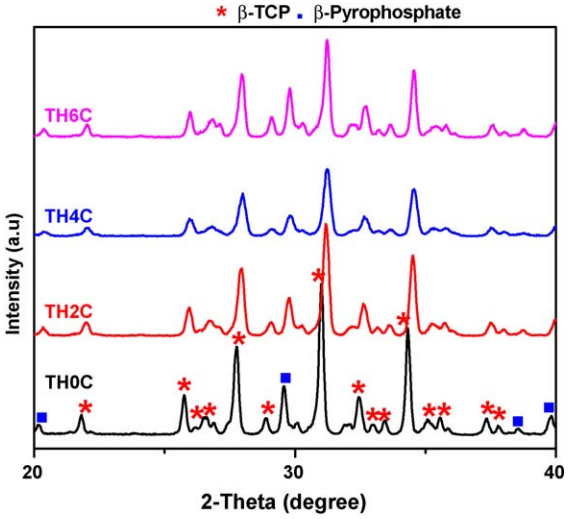

Fig. 2. XRD pattern of calcined samples of material.

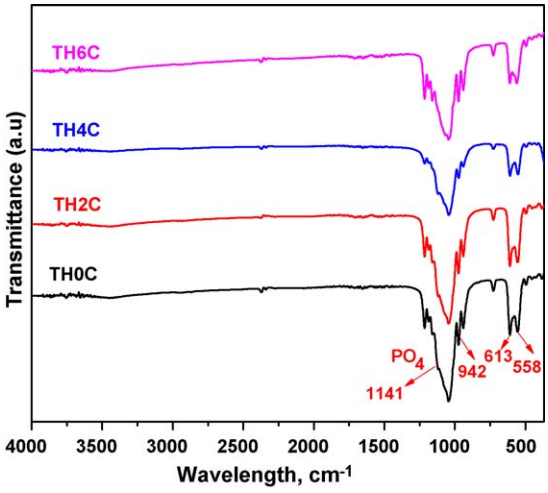

Fig. 4. FT-IR spectra of calcined samples of material.

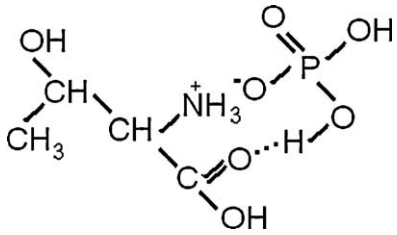

Fig. 5. Threonine and phosphate complex.

band of HPO_4^{2-} appears at 960 cm^{-1} and is attributed to OCP, DCP and Ca-deficient HA The two sharp adsorption bands of PO_4^{3-} appear at 560 and 600 cm^{-1} suggesting that the particle has a crystallized OCP structure [39,40], which is confirmed by the XRD analysis. Furthermore, the adsorption bands due to COO^- are present at 1600–1250 cm^{-1} for OCP. These observations indicate that replaceable HPO_4^{2-} in the hydrated layer was replaced by carboxyl ions [$^-$OOC-R-COO^-] [41].

The FT-IR spectrum of the powders calcined at 900 °C (Fig. 4) become similar to that of β-TCP [42], which is confirmed by the previous XRD result. The characteristic peaks of PO_4 ions, which consist the standard spectra of β-TCP, appear at 942–1141 and 558–613 cm^{-1}. This result is similar to Zhang et al. [43].

The chemical structure of threonine (2-amino 3-hydroxy butanoic acid) and the equilibrium followed Eq. (1).

$$CH_3\text{-}CH(OH)\text{-}CH(NH_3^+)\text{-}COOH \underset{H^+}{\overset{OH^-}{\rightleftarrows}} CH_3\text{-}CH(OH)\text{-}CH(NH_2)\text{-}COO^- \quad (1)$$

In our experimental conditions before the addition of ammonia solution, the initial pH is ∼3.3. After the addition of ammonia solution, the pH rises and the results are shown in Table 1. The two ionic forms of threonine and phosphate species that are formed under these conditions are CH_3-CH(OH)-$CH(NH_3^+)$-COOH and $H_2PO_4^-$, correspondingly, which is possible to create together the complex depicted in Fig. 5. In this complex, one hydroxyl group of phosphate is bonded with the threonine molecule by a hydrogen bond. By this way, this hydroxyl group is protected and remains as acid phosphate group, consequently promotes the precipitation of OCP and DCP, while the threonine molecules are incorporated with the phosphate molecules.

Fig. 6 shows typical SEM micrographs of uncalcined samples. It seems that some particles are consisted of a number of fine grains. The TH0 sample is composed of aggregate particles with no specific shape. After using different concentrations of threonine, a change in shape and size is observed for all samples. By using small concentration of threonine, TH2 sample were composed of numerous isolated small needle-like particles without any agglomeration. As it can be seen from SEM micrographs (Fig. 6), the mean particle size is about 1 μm for sample TH2. TH4 sample were aggregated in spheroidal particles. For TH6 sample, the synthesized particles were big aggregates of round spherical shape and some particles get rod-shaped and their mean diameters were about 1–1.5 μm.

After calcination at 900 °C (Fig. 7), the primary particles were conglomerated tightly into secondary powders of botryoidal (resembling a cluster of grapes in form) shape.

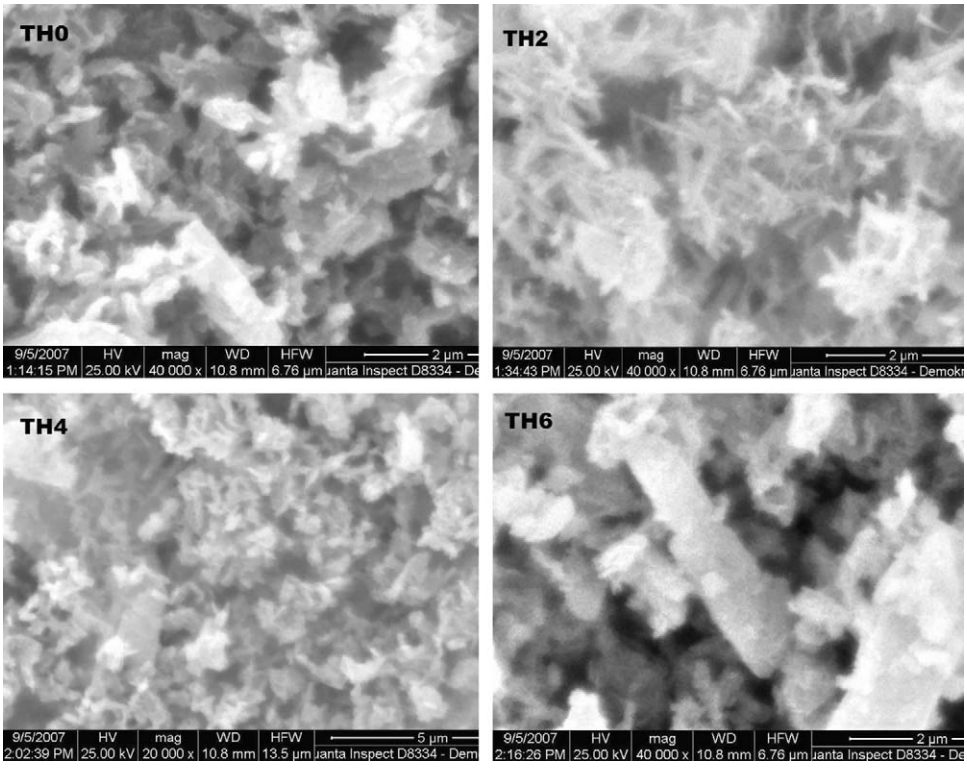

Fig. 6. SEM micrographs of uncalcined samples of material.

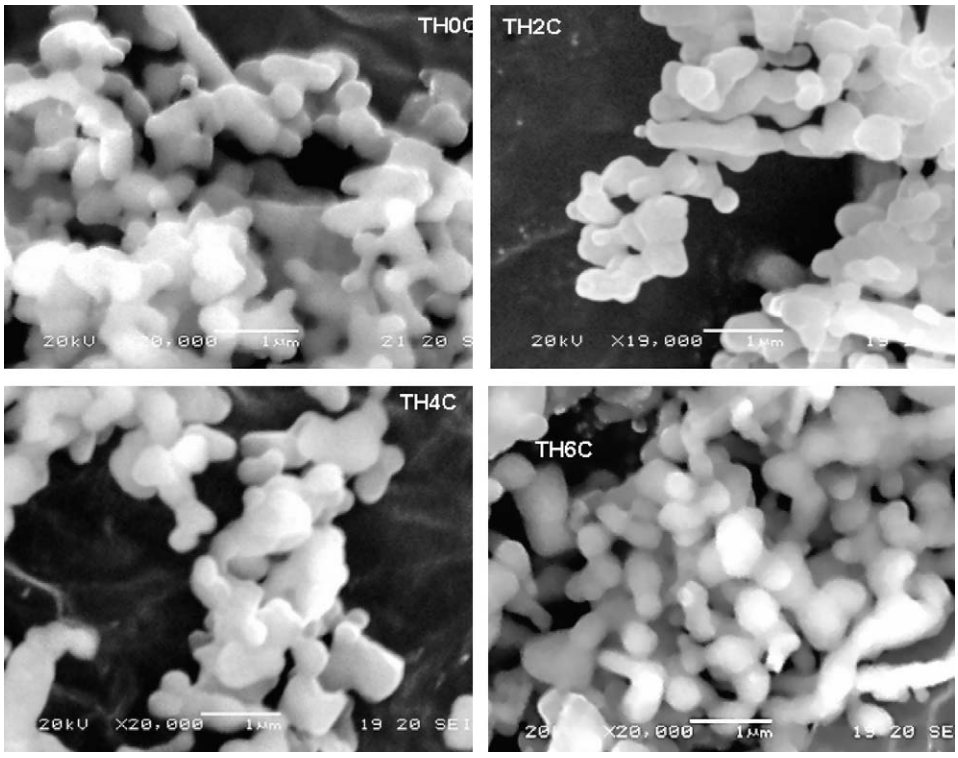

Fig. 7. SEM micrographs of calcined samples of material.

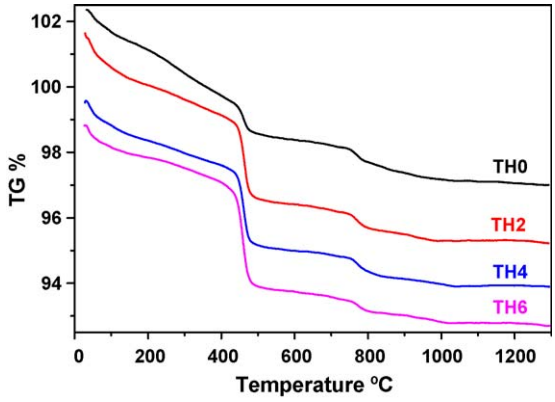

Fig. 8. TG curve of uncalcined samples.

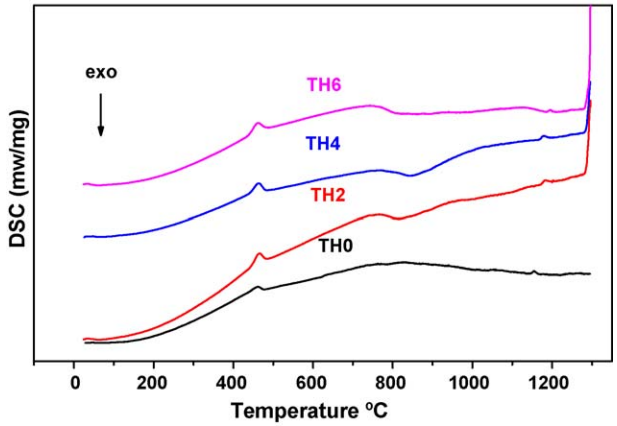

Fig. 9. DSC curve of uncalcined samples.

Calcination did not cause any change in the particles' morphology, and the particles remain in spherical geometry, and kept aggregated. All of these observations suggest that the material formed, in this study, incorporated organic compounds in the interlayer.

Figs. 8 and 9 show the TG and DSC curves of uncalcined samples respectively. The thermal decomposition takes place through four distinguished steps between the temperature ranges 20 until 1300 °C. The first step takes place between room temperature and about 400 °C. This step mainly assigned to the removal of adsorbed and crystalline water (reaction (2)).

$$Ca_8(HPO_4)_2(PO_4) \cdot 5H_2O \rightarrow Ca_8(HPO_4)_2(PO_4) + 5H_2O \quad (2)$$

The second step is endothermic and occurs in temperature area between 400 and 750 °C. In this area occurs mainly the decomposition of octacalcium phosphate to pyrophosphate and TCP (reaction (3)) and monetite (reaction (4)).

$$Ca_8(HPO_4)_2(PO_4) \rightarrow 2Ca_3(PO_4)_2 + Ca_2P_2O_7 + H_2O \quad (3)$$

$$2CaHPO_4 \rightarrow Ca_2P_2O_7 + H_2O \quad (4)$$

In this step the sample TH0, has the lowest mass loss comparing to other samples. The presence of threonine in the solution results to an increase of the mass loss about three times.

In the third step hydroxyapatite and calcium pyrophosphate react, to form β-TCP (reaction (5)), which is the main phase of samples after calcination, as is confirmed from XRD results.

$$Ca_{10}(PO_4)_6(OH)_2 + Ca_2P_2O_7 \rightarrow 4Ca_3(PO_4)_2 + H_2O \quad (5)$$

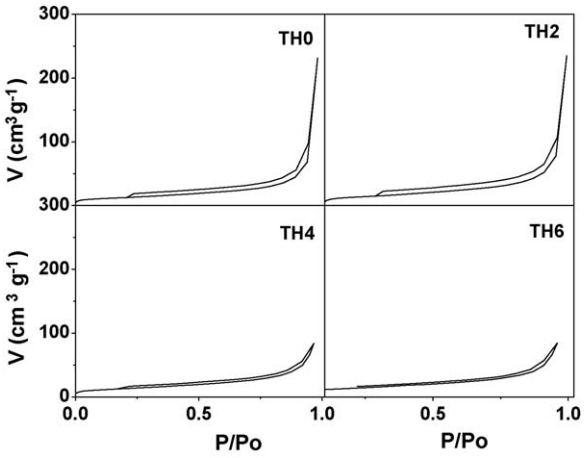

Fig. 10. BET isotherm curves of uncalcined samples of material.

The fourth and final step occurs in temperature range between 1100 and 1300 °C. In this step, the partial dehydroxylation and decomposition of hydroxyapatite took place. The small peaks at about 1200 °C on DSC curves indicate the transformation of β-TCP to α-TCP. At about 1300 °C a sharp endothermic tendency observed on DSC curves for samples TH2, TH4 and TH6, which indicates the melting of calcium pyrophosphate. In sample TH0, though, this peak is not detected due to the absence of pyrophosphate. This observation indicates the consumption of all pyrophosphate amounts according to reaction (5). At the end of the experiment, we observed partial sintering of materials due to melting of pyrophosphates.

The N_2 adsorption–desorption isotherms for samples are shown in Figs. 10 and 11 respectively. The specific surface area is determined by using the BET method [44]. The initial part of the adsorption isotherm ($P/P_0 < 0.2$) corresponding to monolayer and multilayer formation and followed the same path as that given by a corresponding nonporous solid, which support the typical, type II isotherm (IUPAC) for samples TH0, TH2, TH4 and TH6. The hysteresis loops, which occurred between 0.2 and 1.0 relative pressures, are very close to type H3 (IUPAC). Table 1 shows the specific surface area (ssa $m^2\ g^{-1}$)

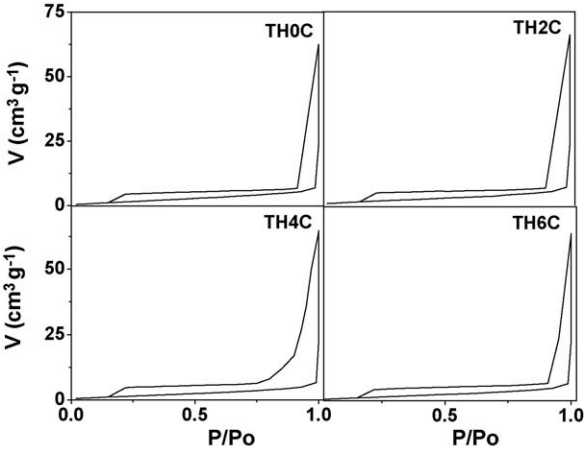

Fig. 11. BET isotherm curves of calcined samples of material.

estimated according to the standard BET method and I-point method [45]. These two methods have very small difference in the results. As we can see from Fig. 10, that relative volume starts between 0 and 10 and the specific surface are (ssa) found from BET equation is between 45 and 53 $m^2\ g^{-1}$ for uncalcined samples (TH0, TH2, TH4 and TH6) and 5–6 $m^2\ g^{-1}$ for calcined samples (TH0C, TH2C, TH4C and TH6C), which indicates that all samples are nonporous. The dramatically decrease of ssa after calcination is in accordance to the SEM observations and indicates a strong sintering process.

4. Conclusion

We have successfully produced calcium phosphate materials by using modified precipitation (pH shock wave) method with high-speed dispersing equipment and the following observations are made:

(1) From XRD patterns for the samples, three phases of OCP, monetite and HA were detected and the lattice parameters for OCP were $a = 10.733$ Å, $b = 13.753$ Å and $c = 5.832$ Å (orthorhombic $Pna\bar{2}1$). For the calcined samples of the same ratio of Ca/P two phases of β-TCP and β-$Ca_2P_2O_7$ were detected and the calculated lattice parameters for β-TCP were $a = 8.174$ Å, $b = 3.348$ Å and $c = 11.394$ Å. The system is monoclinic with the space group $P2/C$.
(2) FT-IR showed the characteristics peak for P–O, HPO_4^{2-} and PO_4^{3} bands.
(3) SEM analysis showed the different morphology of particles. For uncalcined samples of materials, the particle shape was not specific and after used different concentrations of threonine, the shape changed to needle-like, spheroidal and big aggregate of round spherical. On the contrary, all calcined samples of materials showed the same botryoidally shape of particles.
(4) The thermal analysis was studied between temperatures 20 and 1300 °C. The transformation took place through four distinguished steps. At higher temperature, ∼900 °C, β-TCP is formed together with β-$Ca_2P_2O_7$. At the end of the thermal experiment, we observed partial sintering of materials due to the pyrophosphate melting.
(5) The N_2 adsorption–desorption isotherms for the samples were measured by using BET equation and the observed specific surface areas (ssa) were 45–53 m^2/g for uncalcined samples and 5–6 m^2/g for calcined samples.

References

[1] H. Guo, J. Su, J. Wei, H. Kong, C. Liu, Biocompatibility and osteogenicity of degradable Ca-deficient hydroxyapatite scaffolds from calcium phosphate cement for bone tissue engineering, Acta Biomater. 5 (2009) 268–278.
[2] R.L. Spear, R. Tamayev, K.R. Fath, I.A. Banerjee, Templated growth of calcium phosphate on tyrosine derived microtubules and their biocompatibility, Colloid Surf. Sci.: Biointerfaces 60 (2) (2007) 158–166.
[3] S. Nath, R. Tripathi, B. Basu, Understanding phase stability, microstructure development and biocompatibility in calcium phosphate–titania composites, synthesized from hydroxyapatite and titanium powder mix, Mater. Sci. Eng. C 29 (2009) 97–107.

[4] Y. Pekounov, K. Chakarova, K. Hadjiivanov, Surface acidity of calcium phosphate and calcium hydroxyapatite: FTIR spectroscopic study of low-temperature CO adsorption, Mater. Sci. Eng. C 29 (4) (2009) 1178–1181.
[5] X.D. Zhu, H.S. Fan, Y.M. Xiao, D.X. Li, H.J. Zhang, T. Luxbacher, X.D. Zhang, Effect of surface structure on protein adsorption to biphasic calcium-phosphate ceramics in vitro and in vivo, Acta Biomater. 5 (4) (2009) 1311–1318.
[6] G. Graham, P.W. Brown, Reactions of octacalcium phosphate to form hydroxyapatite, J. Cryst. Growth 165 (1996) 106–115.
[7] G.H. Nancollas, Biological Mineralization and Demineralization, Dahlem Konferenzen, Springer-Verlag, Berlin, 1982, pp. 79–99.
[8] X. Lu, Y. Leng, Theoritical analysis of calcium phosphate precipitation in simulated body fluid, Biomaterials 26 (2005) 1097–1108.
[9] J.L. Meyer, E.D. Eanes, A thermodynamic analysis of the secondary transition in the spontaneous precipitation of calcium phosphate, Calcif. Tissue Res. 25 (1978) 209–216.
[10] N. Eidelman, L.C. Chow, W.E. Brown, Calcium phosphate phase transformations in serum, Calcif. Tissue Res. 41 (1987) 18–26.
[11] W.E. Brown, N. Eidelman, B. Tomazic, Octacalcium phosphate as a precursor in biomineral formation, Adv. Dent. Res. 1 (1987) 306–313.
[12] O. Suzuki, M. Nakamura, Y. Miyasaka, M. Kagayama, M. Sakurai, Bone formation on synthetic precursors of hydroxyapatite, Tohoku J. Exp. Med. 164 (1991) 37–50.
[13] O. Suzuki, S. Kamakura, T. Katagiri, M. Nakamuara, B. Zhao, Y. Honda, Bone formation enhanced by implanted octacalcium phosphate involving conversion into Ca-deficient hydroxyapatite, Biomaterials 27 (2006) 2671–2681.
[14] O. Suzuki, M. Nakamuara, Y. Miyasaka, M. Kagayama, M. Sakurai, Maclura pomifera agglutinin-binding glycoconjugates on cnverted apatite from synthetic octacalcium phosphate implanted into subperiosteal region of mouse calvaria, Bone Mine 20 (1993) 151–166.
[15] S. Ban, T. Jinde, J. Hasegawa, Phase transformation of octacalcium phosphate in vivo and in vitro, Dent. Mater. J. 11 (1992) 130–140.
[16] R.Z. LeGeros, G. Daculsi, I. Orly, T. Abergas, W. Torres, Scan. Electron Microsc. 3 (1989) 137–138.
[17] B.B. Tomazic, M.C. Tung, T.M. Gregory, W.E. Brown, Mechanism of hydrolysis of octacalcium phosphate, Scan. Electron Microsc. 3 (1989) 119–127.
[18] M. Iijima, H. Tohda, H. Suzuki, T. Yanagisawa, Y. Moriwaki, Effects of F^- on apatite-octacalcium phosphate intergrowth and crystal morphology in a model system of tooth enamel formation, Calcif. Tissue Int. 50 (1992) 357–361.
[19] M.S. Tung, B. Tomazic, W.E. Brown, The effects of magnesium and fluoride on the hydrolysis of octacalcium phosphate, Arch. Oral Biol. 37 (1992) 585–591.
[20] O. Suzuki, H. Yagishita, M. Yamazaki, T. Aoba, Adsorption of bovine serum albumine onto octacalcium phosphate and its hydrolyzates, Cells Mater. 5 (1995) 45–54.
[21] W. Ballufi, R.M. Allen, S.W. Craig Carter, Kinetics of Materials, Wiley Interscience/A. John Wiley and Sons, Inc., New York, 2005.
[22] R.A. Young, W.E. Brawn, in: G.H. Nancollas (Ed.), Biological Mineralization and Deminaralization, Springer, Berlin, 1992, p. 119.
[23] G.C. Allen, E. Ciliberto, I. Fragala, G. Spoto, Surface bulk study of calcium phosphate bioceramics obtained by metal organic chemical vapor deposition, Nucl. Instr. Methods Phys. 116 (1996) 457–460.
[24] P.T. Cheng, Formation of octacalcium phosphate and subsequent transformation to hydroxyapatite at low supersaturation: a model for cartilage calcification, Calcif. Tissue Int. 40 (1978) 339–343.
[25] M. Iijima, H. Kamemizu, N. Wakamatsu, T. Goto, Y. Doi, Y. Moriwaki, Transition of octacalcium phosphate to hydroxyapatite in solution at pH 7.4 and 37 °C, J. Cryst. Growth 181 (1997) 70–78.
[26] R. Xin, Y. Leng, N. Wang, In situ, TEM examinations of octacalcium phosphate to hydroxyapatite transformation, J. Cryst. Growth 289 (2006) 339–344.
[27] M.J. Arellano-Jiménez, R. García-García, J. Reyes-Gasga, Synthesis and hydrolysis of octacalcium phosphate and its characterization by electron microscopy and X-ray diffraction, J. Phys. Chem. Solids 70 (2009) 390–395.
[28] G.C. Koumoulidis, T.C. Vaimakis, A.T. Sdoukos, Preparation of hydroxyapatite lath-like particles using high-speed dispersing equipment, J. Am. Ceram. Soc. 84 (2001) 1203–1208.
[29] G.C. Koumoulidis, C.C. Trapalis, T.C. Vaimakis, Sintering of hydroxyapatite lath-like powders, J. Therm. Anal. Calorim. 84 (2006) 165–174.
[30] W.H. Elliott, A new threonine metabolite, Biochim. Biophys. Acta 29 (1958) 446–447.
[31] S. Hartshorne, D.M. Greenberg, Studies on liver threonine dehydrogenase, Arch. Biochem. Biophys. 105 (1964) 173–178.
[32] M.I. Bird, P.B. Nunn, Metabolic homoeostasis of L-threonine in the normally-fed rat. Importance of liver dehydrogenase activity, Biochem. J. 214 (1983) 687–694.
[33] R. Guerranti, S. Righi, G. Sandri, E. Panfili, R. Leoncini, E. Marinello, R. Pagani, Intramitochondrial localization of rat liver L-threonine dehydrogenase, Bull. Mol. Biol. Med. 17 (1992) 45–56.
[34] Y.C. Kao, L. Davis, Purification and structural characterization of porcine L-threonine dehydrogenase, Protein Expres. Purif. 5 (1994) 423–431.
[35] Y.W. Chen, E.E. Dekker, R.L. Somerville, Functional analysis of *E. coli* threonine dehydrogenase by means of mutant isolation and characterization, Biochim. Biophys. Acta 1253 (1995) 208–214.
[36] M. Davis, R.E. Austic, Dietary protein and amino acid levels alter threonine dehydrogenase activity in hepatic mitochondria of Gallus domesticus, J. Nutr. 127 (1997) 738–744.
[37] T. Matsumoto, M. Okazaki, M. Inoue, Y. Hamada, M. Tairaa, J. Takahashi, Crystallinity and solubility characteristics of hydroxyapatite adsorbed amino acid, Biomaterials 23 (2002) 2241–2247.
[38] M. Neumann, X-cell – a novel indexing algorithm for routine tasks and difficult cases, J. Appl. Crystallogr. 36 (2003) 356–365.
[39] R.J. Dekker, J.D. de Bruijn, M. Stigter, F. Barrere, P. Layrolle, C.A. van Blitterswijk, Bone tissue engineering on amorphous carbonated apatite and crystalline octacalcium phosphate-coated titanium discs, Biomaterials 26 (2005) 5231–5239.
[40] .B.O. Fowler, M. Markovic, W.E. Brown, Octacalcium phosphate. III. Infrared and Raman vibrational spectra, Chem. Mater. 5 (1993) 1417–1423.
[41] H. Wang, C.J. Lin, R. Hu, F. Zhang, L.W. Lin, A novel nano-micro structured octacalcium phosphate/protein composite coating on titanium by using an electrochemically induced deposition, J. Biomed. Mater. Res. A 87 (2008) 698–705.
[42] S.H. Kwon, Y.K. Jun, S.H. Hong, H. Ee Kim, Synthesis and dissolution behavior of β-TCP and HA/β-TCP composite powders, J. Eur. Ceram. Soc. 23 (2003) 1039–1045.
[43] Y. Zhang, G. Yin, S. Zhu, D. Zhou, Y. Wang, Y. Li, L. Luo, Preparation of β-$Ca_3(PO_4)_2$ bioceramic powder from calcium carbonate and phosphoric acid, Curr. Appl. Phys. 5 (2005) 531–534.
[44] S. Brunauer, H.P. Emmett, E. Teller, Adsorption of gases in multimolecular layers, J. Am. Chem. Soc. 60 (1938) 309–319.
[45] P.J. Pomonis, D.E. Petrakis, A.K. Ladavos, K.M. Kolonia, C.C. Pantazis, A.E. Giannakas, A.A. Leontiou, The I-point method for estimating the surface area of solid catalysts and the variation of C-term of the BET equation, Catal. Commun. 6 (2005) 93–96.